Electronic Supplementary Material (ESI) for Journal of Materials Chemistry A.

Water Bridge Solar Evaporator with Salt-Resistance and Heat Localization for Efficient Desalination

Yu-Qiong Luo [a,b], Fei Song [a,*], Xiu-Li Wang [a], Yu-Zhong Wang [a,*]

[a] The Collaborative Innovation Center for Eco-Friendly and Fire-Safety Polymeric Materials (MoE), National Engineering Laboratory of Eco-Friendly Polymeric Materials (Sichuan), State Key Laboratory of Polymer Materials Engineering, College of Chemistry, Sichuan University, Chengdu 610064, China.

[b] Key Lab for Special Functional Materials of Ministry of Education, School of Materials, Henan University, Kaifeng, Henan Province 475004, China

* Corresponding authors: songfei520@gmail.com; yzwang@scu.edu.cn

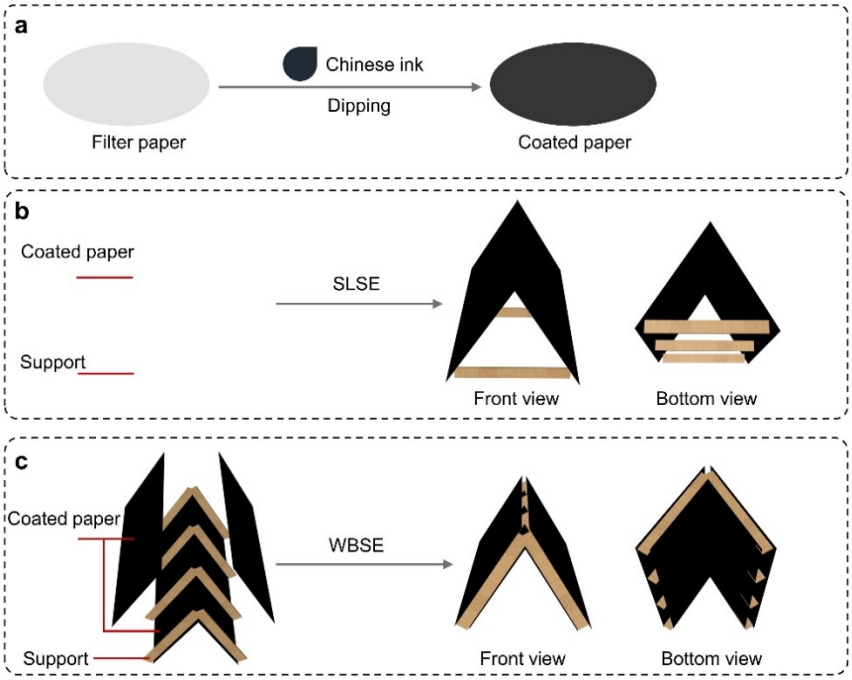

Figure S1. Fabrication process of (a) coated paper, (b) single layered solar evaporator (SLSE) and (c) water-bridge solar evaporator (WBSE).

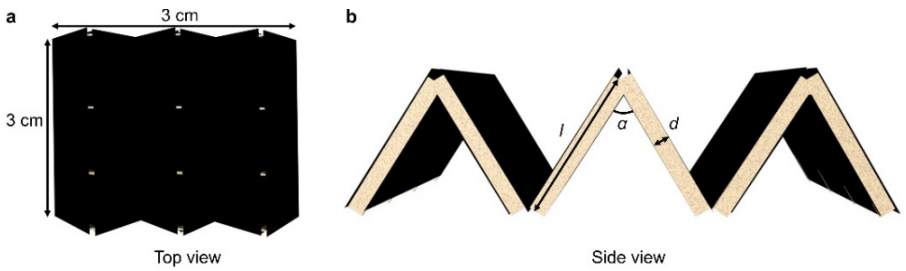

Figure S2. Illustrating geometrical definitions of the WBSE. (a) Top view and (b) Side view of the WBSE. The projection area of the WBSE is 3 × 3 cm^2.

Table S1. WBSE with different side wall length (l), included angle (α) and parallel paper distance (d).

Samples	Side wall length (l: cm)	Parallel paper distance (d: mm)	Included angle (α: °)
$WB_{1.5\text{-}40\text{-}1.0}SE$	1.5	1.0	40
$WB_{1.3\text{-}46\text{-}1.0}SE$	1.3	1.0	46
$WB_{1.3\text{-}46\text{-}0.5}SE$	1.3	0.5	46
$WB_{1.3\text{-}46\text{-}2.0}SE$	1.3	2.0	46
$WB_{1.3\text{-}34\text{-}1.0}SE$	1.3	1.0	34
$WB_{1.3\text{-}72\text{-}1.0}SE$	1.3	1.0	72

Figure S3. A white foam with area of 3×3 cm^2 is selected to subtract out the effect of exposed area in the evaporation device.

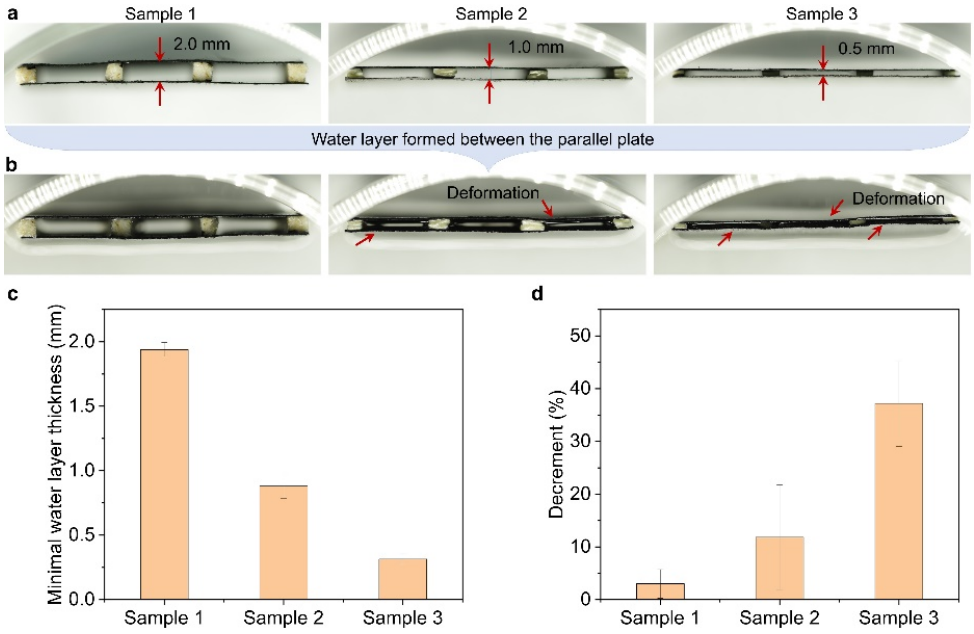

Figure S4. Capillary deformation of the parallel coated paper. (a) Photograph of parallel paper with different distance (Sample 1: 2.0 mm, Sample 2: 1.0 mm and Sample 3: 0.5 mm). (b) Photograph of the parallel paper with elevated water layer. The two filter papers are drawn closer due to capillary force, which is more obvious for sample 3. (c) Minimal water layer thickness and (d) Parallel paper distance decrement of different samples. Parallel paper with smaller distance exhibits larger capillary force, inducing larger distance decrement.

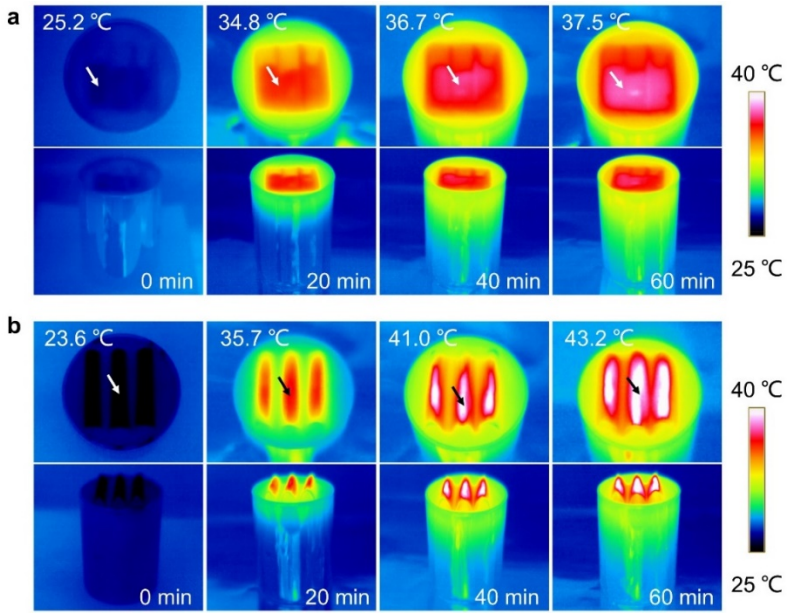

Figure S5. IR camera images of the (a) flat evaporator and (b) SLSE over 60 min irradiation under one-sun. Surface temperature of the flat evaporator increase from 25.2 °C to 37.5 °C after 60 min evaporation. High surface temperature on the SLSE top (43.2 °C) is observed, which is caused by salt precipitation. Those IR camera images were recorded by an IR camera (Fluke Tix580).

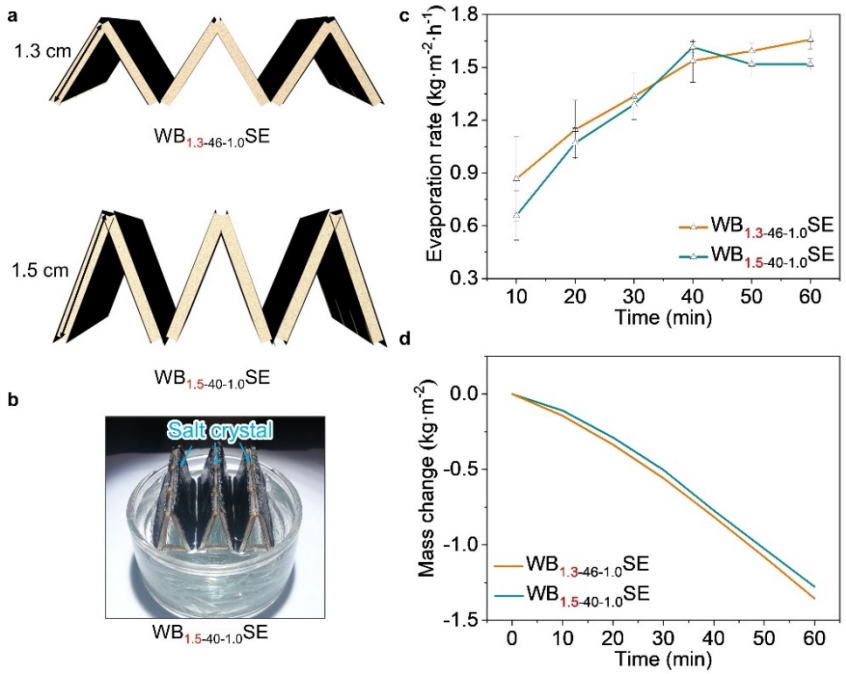

Figure S6. Evaporation performance of the WBSE with different side wall length (*l*) in 3.5 wt% brine for 60 min under one-sun. (a) Schematic diagram of the $WB_{1.5\text{-}40\text{-}1.0}SE$ and $WB_{1.3\text{-}46\text{-}1.0}SE$. (b) Salt deposition is observed on the $WB_{1.5\text{-}40\text{-}1.0}SE$ after 60 min evaporation. (c) Evaporation rate and (d) mass change of the $WB_{1.5\text{-}40\text{-}1.0}SE$ and $WB_{1.3\text{-}46\text{-}1.0}SE$. Due to salt deposition, the $WB_{1.5\text{-}40\text{-}1.0}SE$ shows a high evaporation rate of 1.62 kg m^{-2} h^{-1} at 40 min and decreases to 1.52 kg m^{-2} h^{-1} at 60 min.

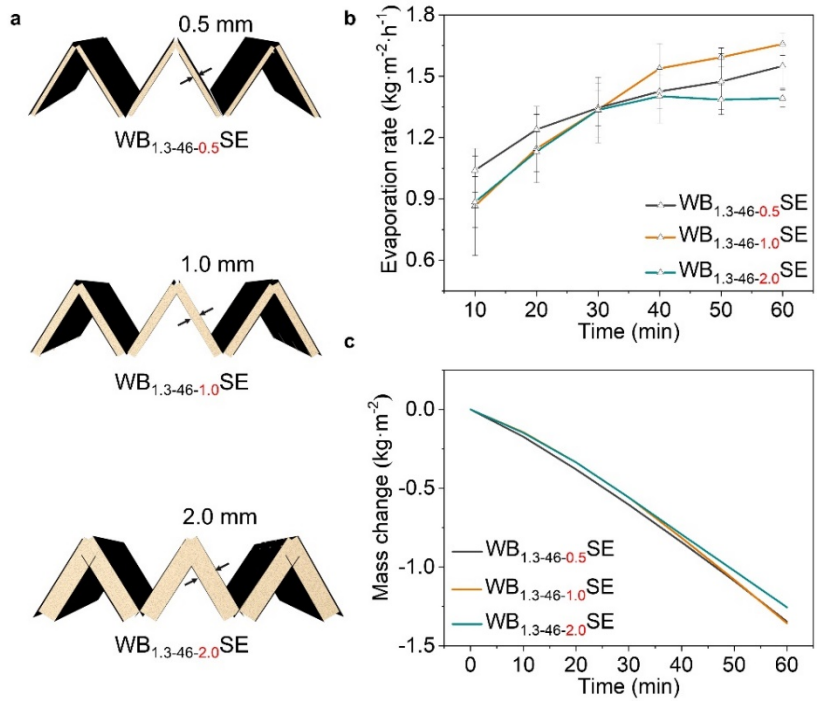

Figure S7. Evaporation performance of the WBSE with different parallel paper distance (*d*) in 3.5 wt% brine for 60 min under one-sun. (a) Schematic diagram of the $WB_{1.3\text{-}46\text{-}0.5}SE$, $WB_{1.3\text{-}46\text{-}1.0}SE$ and $WB_{1.3\text{-}46\text{-}2.0}SE$. (b) Evaporation rate and (c) mass change of the WBSE. The $WB_{1.3\text{-}46\text{-}0.5}SE$ shows comparable evaporation performance with the $WB_{1.3\text{-}46\text{-}1.0}SE$ in 3.5 wt% brine.

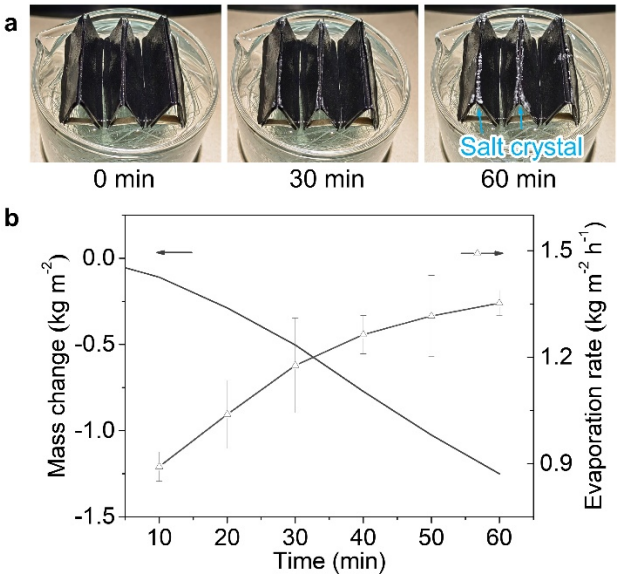

Figure S8. Evaporation performance of the $WB_{1.3\text{-}46\text{-}0.5}SE$ in 20 wt% brine for 60 min under one-sun. (a) Salt precipitation is observed on the $WB_{1.3\text{-}46\text{-}0.5}SE$ after 60 min evaporation. (b) Mass change and evaporation rate of the $WB_{1.3\text{-}46\text{-}0.5}SE$. The evaporation rate and mass change of the $WB_{1.3\text{-}46\text{-}0.5}SE$ at 60 min is 1.35 kg m^{-2} h^{-1} and 1.25 kg m^{-2}, respectively.

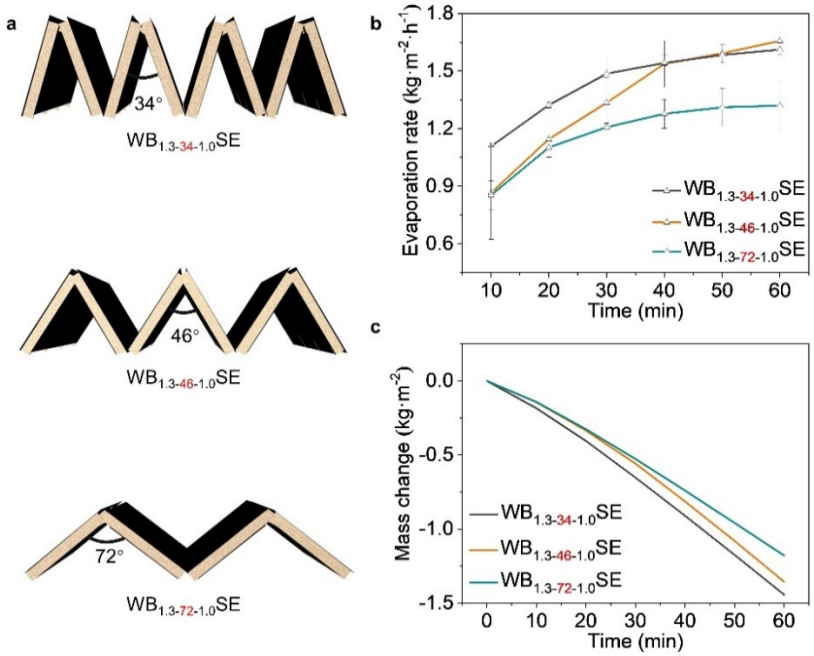

Figure S9. Evaporation performance of the WBSE with different included angle (α) in 3.5 wt% brine for 60 min under one-sun. (a) Schematic diagram of the $WB_{1.3\text{-}34\text{-}1.0}SE$, $WB_{1.3\text{-}46\text{-}1.0}SE$ and $WB_{1.3\text{-}72\text{-}1.0}SE$. (b) Evaporation rate and (c) mass change of the WBSE. Due to large specific surface areas, $WB_{1.3\text{-}34\text{-}1.0}SE$ and $WB_{1.3\text{-}46\text{-}1.0}SE$ show higher evaporation rate than $WB_{1.3\text{-}72\text{-}1.0}SE$.

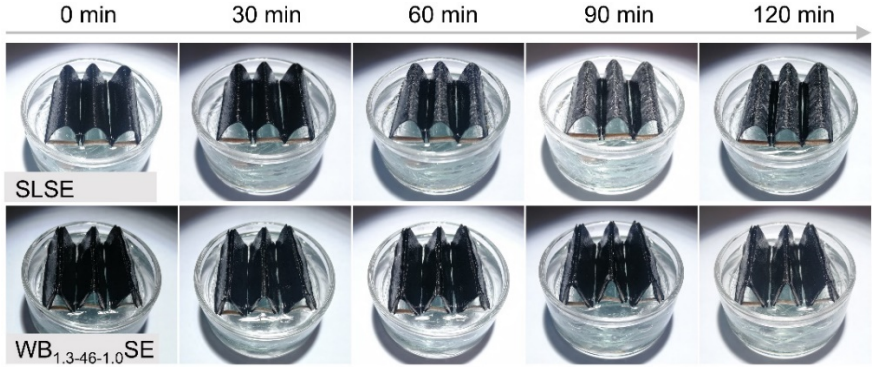

Figure S10. Photographs of the SLSE and $WB_{1.3\text{-}46\text{-}1.0}SE$ over time for solar desalination (15 wt%) under one-sun. The SLSE surface is covered by salt crystals at 120 min, while no salt crystal is observed on the $WB_{1.3\text{-}46\text{-}1.0}SE$ surface.

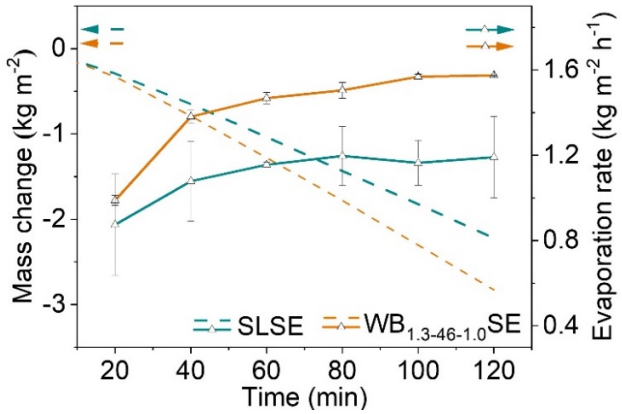

Figure S11. Mass change and evaporation rate of different samples in 15 wt% brine. The mass change and evaporation rate of the $WB_{1.3\text{-}46\text{-}1.0}SE$ is higher than that of the SLSE.

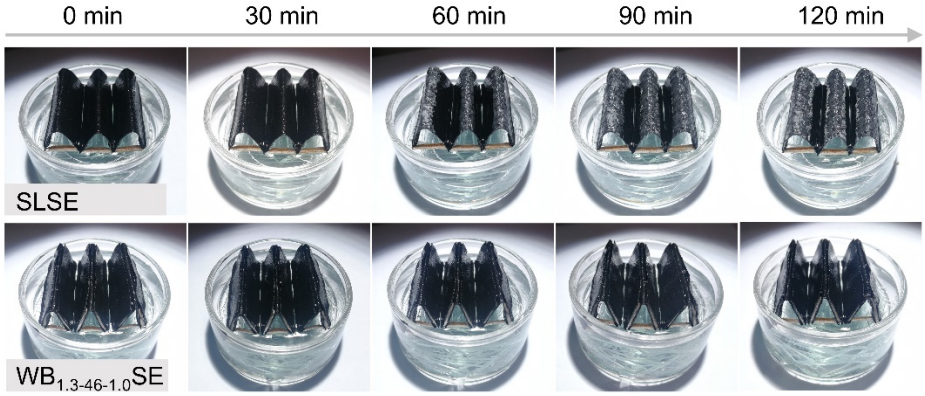

Figure S12. Photographs of the SLSE and $WB_{1.3\text{-}46\text{-}1.0}SE$ over time for solar desalination (20 wt%) under one-sun. The SLSE surface is covered by salt crystals at 120 min, while no salt crystal is observed on the $WB_{1.3\text{-}46\text{-}1.0}SE$ surface.

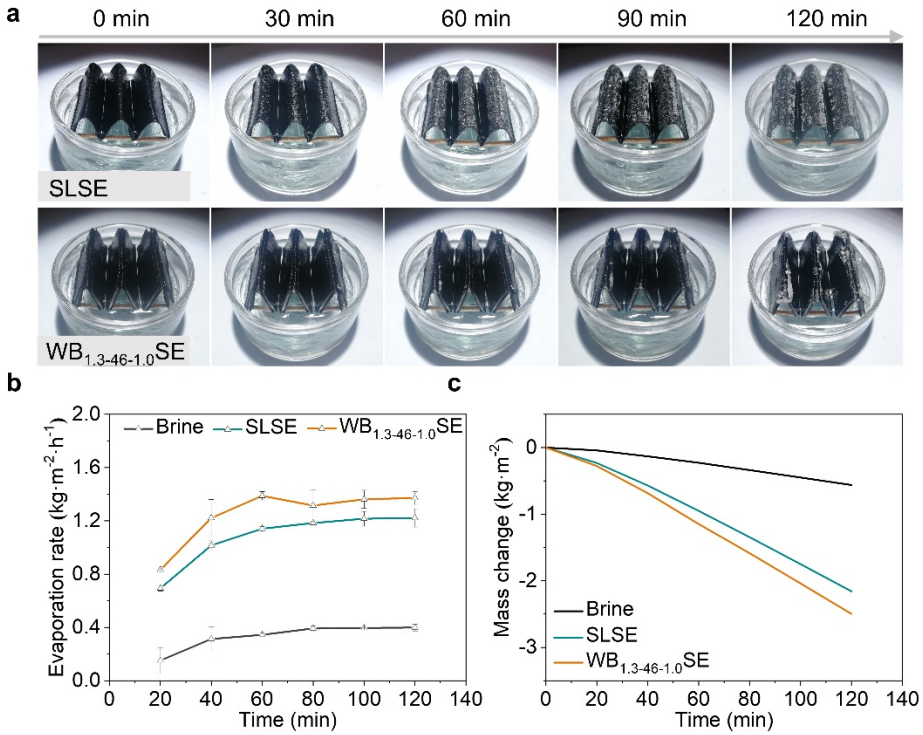

Figure S13. Evaporation performance of the SLSE and $WB_{1.3\text{-}46\text{-}1.0}SE$ in 25 wt% brine under one-sun. (a) Photographs of SLSE and $WB_{1.3\text{-}46\text{-}1.0}SE$ over time for solar desalination (25 wt%). Both of the SLSE and $WB_{1.3\text{-}46\text{-}1.0}SE$ surface are covered by salt crystals at 120 min. (b) Evaporation rate and (c) Mass change of different samples. Due to salt deposition, evaporation rate of the $WB_{1.3\text{-}46\text{-}1.0}SE$ decreases to 1.37 kg m^{-2} h^{-1} at 120 min.

Heat loss analysis

The heat loss in $WB_{1.3\text{-}46\text{-}1.0}SE$ consists of three parts: radiation loss, conduction loss and convection loss, as analyzed below [1-5].

a. Radiation loss:

The radiation loss is calculated according to the Stefan-Boltzmann equation,

$$\Phi = \varepsilon A\sigma\left(T_1^4 - T_2^4\right) \quad \text{(S1)},$$

$$\text{Radiation loss}=\frac{\Phi}{AC_{\text{opt}}q_{\text{i}}}=\frac{\varepsilon\sigma\left(T_1^4 - T_2^4\right)}{C_{\text{opt}}q_{\text{i}}} \quad \text{(S2)},$$

where Φ represents the heat flux, ε denotes the emissivity which is assumed to be 1 here, A is the evaporation surface area (9 cm^2), σ represents the Stefan-Boltzmann constant which is 5.67×10^{-8} J m^{-2} s^{-1} K^{-4}, T_1 is the surface temperature of the evaporator under 1 kw m^{-2} solar illumination. T_2 is the temperature of adjacent environment. T_1 and T_2 were monitored by thermocouple (LINI-T UT320D). After 60 min evaporation, T_1 and T_2 are 307.2±1.1 K (34.2±1.1 °C) and 311.7 ±1.1 K (38.7±1.1 °C), respectively. C_{opt} represents the optical concentration of the solar which is 1 here, q_i is the nominal solar illumination (1 kW m^{-2}). Therefore, the radiation loss is calculated to be -3.02% for our evaporator under one sun.

b. Conduction loss:

The conduction loss is calculated based on the bulk water absorption heat as following,

$$Q = mC\Delta T \quad \text{(S3)},$$

$$\text{Conduction loss}=\frac{Q}{AC_{\text{opt}}q_{\text{i}}\Delta t}=\frac{mC\Delta T}{AC_{\text{opt}}q_{\text{i}}\Delta t} \quad \text{(S4)},$$

where Q denotes the heat flux, m represents the mass of the bulk water solution, C is the specific heat capacity of water which is 4.2 kJ $°C^{-1}$ kg^{-1}, ΔT represents temperature change of the bulk solution during the period of Δt (1 h). In this work, m = 25.0 g, ΔT = 1.05 °C under one sun. Accordingly, the heat loss of conduction is calculated to be 3.4%.

c. Convection loss:

The convection loss is calculated by the Newton's Law of Cooling as below,

$$\psi = \xi A\Delta T \quad \text{(S5)},$$

$$\text{Convection loss}=\frac{\psi}{AC_{\text{opt}}q_{\text{i}}}=\frac{\xi\Delta T}{C_{\text{opt}}q_{\text{i}}} \quad \text{(S6)},$$

where ψ is the thermal energy, ξ represents the convection heat transfer coefficient which is set to be 10 J m^{-2} s^{-1} K^{-1} here, ΔT represents the temperature difference between the surface temperature of the evaporator and the adjacent environment temperature. Thus, we could calculate the heat loss of convection was -4.5 % of all received energy.

The temperature of the $WB_{1.3\text{-}46\text{-}1.0}SE$ and adjacent air is 34.2 and 38.7 °C after 60 min irradiation (Figure 4e and thermocouple detecting result). In this case, the $WB_{1.3\text{-}46\text{-}1.0}SE$ will take energy from the environment. Based on the above analysis, the radiation loss,

conduction loss and convection loss is calculated to be -3.02%, 3.4% and -4.5 %, respectively. The total heat loss of the steam generation system is -4.12% under one sun, representing a solar-to-vapor conversion efficiency of 104.12%.

References

1. Z. X. Wang, T. Horseman, A. P. Straub, N. Y. Yip, D. Y. Li, M. Elimelech and S. H. Lin, *Sci. Adv.*, 2019, **5**, eaax0763.
2. G. Ni, G. Li, S. V. Boriskina, H. X. Li, W. L. Yang, T. J. Zhang and G. Chen, *Nat. Energy*, 2016, **1**, 1-7.
3. Y. D. Kuang, C. J. Chen, S. M. He, E. M. Hitz, Y. L. Wang, W. T. Gan, R. Y. Mi and L. B. Hu, *Adv. Mater.*, 2019, **31**, 1900498.
4. L. F. Cui, P. P. Zhang, Y. K. Xiao, Y. Liang, H. X. Liang, Z. H. Cheng and L. T. Qu, *Adv. Mater.*, 2018, **30**, 1706805.
5. H. Song, Y. Liu, Z. Liu, M. H. Singer, C. Li, A. R. Cheney, D. Ji, L. Zhou, N. Zhang, X. Zeng, Z. Bei, Z. Yu, S. Jiang and Q. Gan, *Ad. Sci.*, 2018, **5**, 1800222.